Numerical and Experimental Simulation of Extreme Operational Conditions for Horizontal Axis Wind Turbines Based on the IEC Standard

Kamran Shirzadeh [1,2], Horia Hangan [1,3], Curran Crawford [1,4]

[1] WindEEE Research Institute, University of Western Ontario, London, Ontario, N6M 0E2, Canada
[2] Mechanical and Material Engineering, Western University, London, N6A 3K7, Canada
[3] Civil and Environment Engineering, Western University, London, N6A 3K7, Canada
[4] Mechanical Engineering, Victoria University, Victoria, V8W 2Y2, Canada

Correspondence: Kamran Shirzadeh (kshirzad@uwo.ca)

Abstract. In this study, the possibility of simulating some transient and deterministic extreme operational conditions for horizontal axis wind turbines based on the IEC 61400-1 standard in the Wind Engineering, Energy and Environment (WindEEE) Dome at Western University was investigated. There are 60 fans (a matrix of 4 by 15 with 0.8m diameter each) on one of the walls of this hexagonal wind tunnel for creating straight flows which the power set-points for each fan can be specified individually. In addition, these fans have adjustable Inlet Guiding Vanes (IGV) that can be controlled uniformly across all of the fans. Using these capabilities, experiments were carried out for the Extreme Operational Gust (EOG), positive and negative Extreme Vertical Shear (EVS), and Extreme Horizontal Shear (EHS) cases, tailored for a 2.2 m HAWT scaled turbine. This study started by developing a numerical model for the test chamber, then using it to tune the fan setups for each extreme condition with proper scaling. Physical experiments then carried out using those settings, then a comparison made between the flow field time history and the prescribed conditions from the standard. The comparisons show promising results, this can be a contribution to future scholars investigating the interaction of the HAWT with these conditions in physical experiments.

1. Introduction

Wind energy is one of the primary sources of low carbon energy for mitigating the global increasing energy demand. However, one of the basic factors for this market to thrive is continued lowering of the levelized cost of electricity (LCOE), which is enhanced by ensuring the life of the wind energy systems is reliably long (Ueckerdt et al., 2013). Having a long life cycle for these energy systems dramatically increases the probability of them encountering various extreme weather and wind conditions (Patlakas et al., 2017). Therefore, the design of wind energy systems must consider extreme environmental conditions with statistically accurate return periods. The International Electrotechnical Commission (IEC) has some deterministic design codes for commercial Horizontal Axis Wind Turbines (HAWT) in operating conditions, specifically in IEC 61400 part one (1999). In the second edition of standard, two return periods for extreme conditions during turbine operation were included: 1 and 50-years. The third edition of the standard removed the 50-years return period (2005). The

most recent fourth edition of the standard (2019) has continued the standard's trend in prescribed analysis toward use of statistical analysis and extrapolation of load cases, however the use of the second edition of the standard is justified in this work presented here owing to the incremental development of a gust loading experimental capability, rather than trying to replicate the much more complex current standard. The work is a logical progression from steady state wind tunnel rotor testing that has been the norm to date in experimental campaigns.

One of the extreme cases in the standard is the extreme operational gust (EOG). A gust is defined as a sudden increase in velocity over its mean value, which is a transient feature of a turbulent wind field (Tony Burton, Nick Jenkins, David Sharpe, 2011).These turbulent features in the Atmospheric Boundary Layer (ABL) depend on topography, surface roughness, obstacles up-stream of the turbine, thermal stability (Suomi et al., 2013) and mesoscale climactic systems such as thunderstorms and downbursts (Chowdhury et al., 2018). In theory for different application there are various simplified models of gust based on a peak factor and the whole rising and falling time in the wind speed. The peak factor is the ratio of the peak velocity (maximum or minimum) and the average wind speed. Wind gusts can happen over various length and time scales in nature. The most damaging gusts for any type of structures are the ones that have the same length scale or envelope the whole structure (Hu et al., 2018). Smaller gusts, relative to the wind turbine size, causes fatigue loads on blades and can include the 'gust slicing effect'. These small gusts also can cause instabilities in the power output of wind turbine generators. For a small electricity network, these instabilities in power generation can cause serious problems for managing power transmission and distribution. The worst case is when a peak gust wind speed is higher than the wind turbine cut-out speed, which if prolonged enough can cause the control system to abruptly stop the wind turbine (Hansen, 2015). From an aerodynamic point of view, gusts can result in undesired acceleration of the rotor and drivetrain. The most reasonable solution would be an adjustable generator load or adjusting blade pitch angles after detection of the gust (Pace et al., 2015; Lackner and Van Kuik, 2010). Developing LIDAR technology can make a substantial contribution in controlling the wind turbine by measuring the wind field upstream, thereby giving enough time for the control system to react properly (Schlipf et al., 2013; Bossanyi et al., 2014).

In addition to uniform gusts, the standard specifies deterministic Extreme Vertical and Horizontal Shears (EVS, EHS). These shears can induce asymmetric loads on the rotor which are in turn transferred into the whole structure. The vertical shears can induce tilting or out-of-plane moments on the rotor and nacelle (Micallef and Sant, 2018). In a positive vertical shear, the blade moving at higher heights could experience stall while the one moving at lower height will experience a reduction in overall angle of attack relative to design condition (and vice versa for negative vertical shear) (Sezer-Uzol and Uzol, 2013). If extreme enough, the blades may experience a phenomenon known as dynamic stall (Hansen, 2015; Gharali and Johnson, 2015). All these together will result in instability and reduction in power generation, as well as highly dynamic fatigue loads on the system (Jeong et al., 2014; Shen et al., 2011). The effects of horizontal shear are similar to vertical shear in terms of power performance and blade fatigue loads. However, EHS also induces yaw moments on the whole structure. These transient shears can happen for similar reasons as uniform gusts, but mostly happen within wind farms, where the wind

turbines sometimes operated in the wakes of other operating up-stream wind turbines (Thomsen and Sørensen, 1999),
70   (González-Longatt et al., 2012).

This standard also defines a classification for commercial wind turbines based on a reference wind speed and turbulence intensity, in a way that covers most on-shore applications. The Turbulence Intensity (TI) is defined as the ratio of the standard deviation of wind speed fluctuations to the mean 10 min averaged wind speed. TI levels of 16%, 14% and 12% correspond to A, B and C turbulence classes. For velocity references, 3 classes have been defined (I, II, III) corresponding to
75   50, 42.5, 37.5 m/s wind speeds, with one further class for special conditions (e.g. off-shore and tropical storms) which should be specified by the designer. The design turbulence standard deviation for the stream wise direction in the standard is defined by a normal turbulence model:

$$\sigma_u = I_{ref}(0.75V_{hub} + b); \quad b = 5.6 \frac{m}{s}, \tag{1}$$

The V_{hub} is the average wind velocity at the at hub-height. The EOG with $t = 0$ at the beginning of the gust, is defined as:

$$V(t) = \begin{cases} \bar{V} - 0.37\beta \left(\dfrac{\sigma_u}{1 + 0.1\left(\dfrac{D}{\Lambda_u}\right)} \right) \sin\dfrac{3\pi t}{T}\left(1 - \cos\dfrac{2\pi t}{T}\right); when \quad 0 \le t \le T, \\ \bar{V}; \quad when\ t > T\ or\ t < 0, \end{cases} \tag{2}$$

The factor β takes the value of 4.8 or 6.4 for gusts with recurrence periods of 1 or 50-years respectively. The duration of the
80   gust T is specified as 10.5 s for 1-year and 14 s for 50-years return periods. The D is the diameter of the rotor, and Λ_u is the longitudinal turbulence scale parameter which is a function of the hub height:

$$\Lambda_u = \begin{cases} 0.7Z & for\ Z \le 60m, \\ 42m & for\ Z > 60m, \end{cases} \tag{3}$$

The EVS and EHS have similar equations which can be added to or subtracted from the main uniform or ABL inflow. The EVS can be calculated using the Eq. (4):

85

$$V_{EVS}(Z,t) = \begin{cases} \left(\dfrac{Z - Z_{hub}}{D}\right)\left(2.5 + 0.2\,\beta\sigma_u\left(\dfrac{D}{\Lambda_u}\right)^{0.25}\right)\left(1 - \cos\left(\dfrac{2\pi t}{T}\right)\right); when \quad 0 \le t \le T, \\ 0 \quad ;\ when\ t > T\ or\ t < 0, \end{cases} \tag{4}$$

For a commercial B-III class HAWT with 92 m diameter rotor and 80 m hub height, at 10m/s average velocity, the prescribed EOG and EVS for 1-year return period are presented at Figure 1. The time window in this figure starts and ends with the extreme event, which is 10.5s for 1-year return period. Generally speaking, the peak factor of the EOG decreases
90   with increasing size of the turbine or decreasing hub height, and vice versa for the EVS based on these equations.

| (a) | (b) |
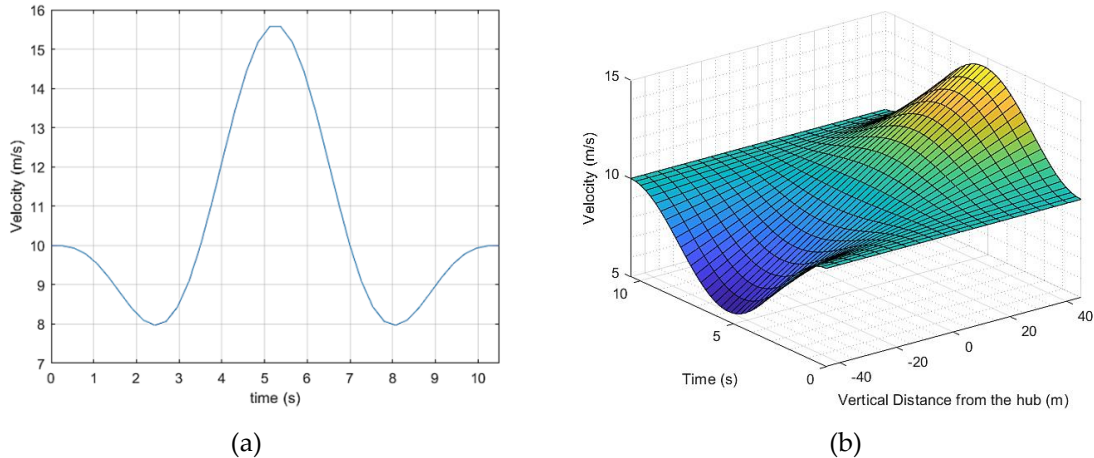
Figure 1: The extreme operational conditions with 1-year return period for a full scale HAWT class B-III with 92m diameter and hub height of 80m at 10 m/s uniform wind speed, (a) extreme operational gust, (b) extreme vertical shear on the rotor with hub height as reference

These extreme models are relatively simple and are not able to capture the true coherent turbulent wind characteristics (Cheng and Bierbooms, 2001). This is the reason for recent editions of the IEC standard to utilize statistical methods for characterizing extreme gust event performance. This has been enabled by computational resources to analysis wind energy systems in dynamic wind environments. Experimental investigations are typically limited to steady state conditions (Snel et al., 2007; Sørensen et al., 2002). Only a limited number of studies have looked at transitory or turbulent wind conditions (Peinke et al.). Developing a method to experimentally test extreme conditions on rotors is a valuable contribution to researchers in this field, and as such is the main motivation and focus of this study examining deterministic transitory gust profile generation.

This paper is organized in three sections beside the introduction and it is as follows. Section 2 details the development of the numerical model for the WindEEE test chamber which was used to obtain the fan setups to use in physical simulation of the gusts. This section also provides a length and time scaling of the gust which based on that the target gusts for experimental campaign are introduced. Section 3 presents the results from velocity measurements at the test section in two parts, firstly the steady shears to double check the accuracy of the developed numerical model to simulate the shear layers and secondly the final transient simulated gusts and their comparison with IEC standard. Section 4 provides the conclusions.

2. Methodology

2.1. WindEEE Dome

The physical experiments were conducted in the WindEEE Dome at Western University, Canada. This is a versatile facility with different modes for creating various three dimensional and non-stationary wind systems (Hangan et al., 2017). It has an

inner test chamber with a 25 m diameter hexagonal footprint and 3.8 m height. A render of the inner shell of the test chamber for straight flows is shown in Figure 2a. The test chamber is in turn surrounded by an outer shell. It has a total 106 fans, including 60 fans installed on one wall and 40 fans over the other five peripheral walls. There are also 6 larger fans in a plenum above the test chamber. A side view schematic of the WindEEE Dome shown at Figure 2b. In general, the

115   arrangement of multiple fans allows for sheared, yawed and circulating flows to be created in the dome. To simulate a straight flow, the louvers at the top and peripheral sides of the test section are closed and the flow goes from the 60 fans to the center of the test section and then through the mesh of the wall at the opposite end, before passing through heat exchangers and recirculating over the top, back to the 60 fans' inlet. Each fan is 0.8 m in diameter with 30 kW nominal maximum power. In order to reach higher velocities and better flow uniformity characteristics at the center of the test

120   chamber, a two-dimensional contraction can be setup to streamline the flow as shown in Figure 2c.

(a)   (b)

(c)
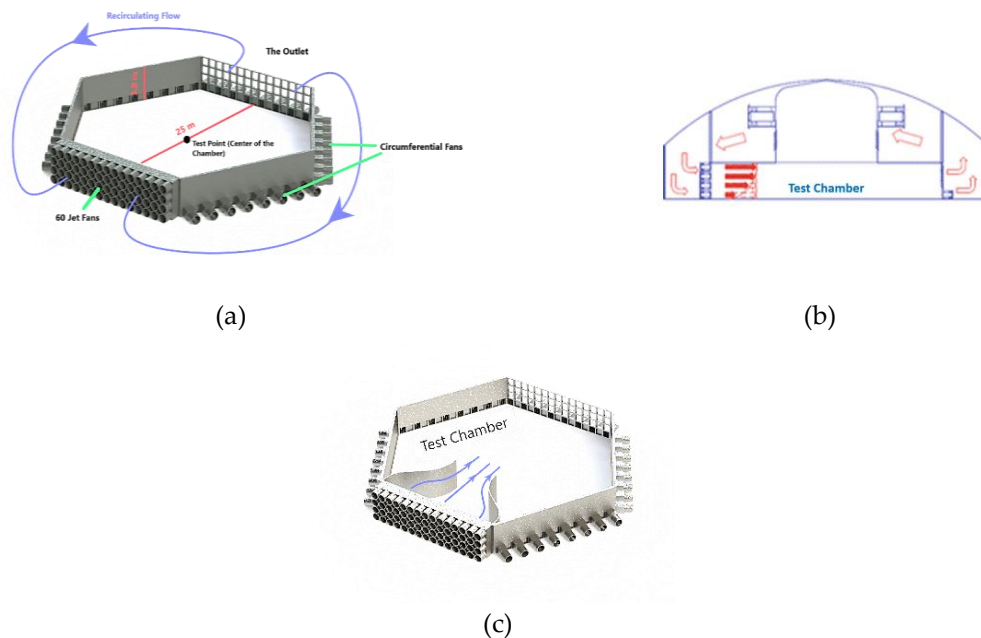
Figure 2. A brief geometry of the WindEEE hexagonal test chamber, (a) render of test chamber and flow path, (b) side view schematic of the WindEEE dome, (c) render of the test chamber with contraction walls

The power set-points of the 60 fans can be adjusted by a spreadsheet file with 60 columns. The numbering of the fans starts with the top left fan, row by row ending with the bottom right fan in Figure 2. The operating software at the facility can read the spread sheet file and switch power set-points as fast as 2 Hz. However, this does not imply the fans themselves can throttle from 0% to 100% power at 2 Hz (due to rotational inertia of the fans and electrical current filtering it takes ~3 s).

125   Another capability at the inlet wall utilizes fans with adjustable inlet guide vanes which can regulate the amount of mass flow through the fans. These vanes can be adjusted uniformly from 0% open (close) to 100% open (Figure 3). They can also be adjusted dynamically by setting an actuation frequency, duty cycle and an initial position. The actuation frequency

specifies the time between two cycles, while the duty cycle specifies the duration of an individual cycle specified as a percentage of the time between two successive cycles.

130

(a)   (b)
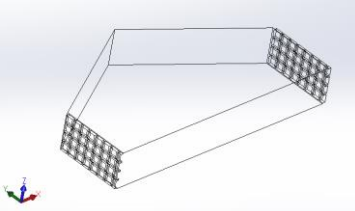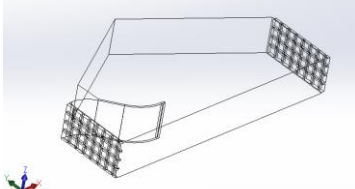
Figure 3. The adjustable vanes at the inlets of the 60 fans wall, (a) 100% open vanes, (b) 70% open vanes

2.2. Numerical Flow Analysis Setup and Tuning/Validation
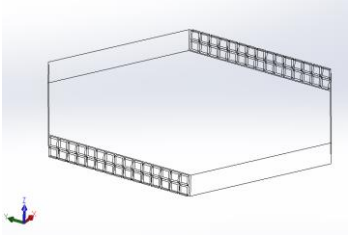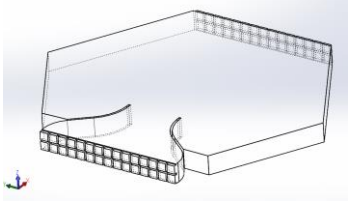
In order to have a better understanding of the flow field in the test chamber, a numerical model for the test chamber was created using the commercial Star-CCM+ CFD software, which helped to predict the fan power setups for different scenarios prior running the experiments.

135 The initial step of the numerical study was to calibrate the boundary condition parameters based on the previous experiment data that were available for scaled ESDU ABL profiles both with and without contraction walls (Hangan et al., 2016). The simulated fan powers were then adjusted to reach the desired average velocity profiles at the test section to match the existing experimental data. For this purpose, simplified symmetrical domains of the test chamber were generated to save considerable CPU time as listed at Table 1. In order to discretize the domains, a mesh was generated using the polyhedral

140 automated mesh function, built-in Star-CCM+ software.

Table 1: The generated domains for simulating different cases with their name tags

Picture of the Domain	Application	Name Tag
	Simulating ABLs and EVS & EOG and tuning the boundary conditions parameters	V
	Simulating ABLs and EVS & EOG with contraction walls and tuning the boundary conditions parameters	V-c

	Simulating EHS	H
	Simulating EHS with contraction walls	H-c

145   The general details for the generated grids are presented in Table 2. For all of the cases, 5 prism layers with a total thickness of 0.05m and with stretching of 30 % at the solid walls with minimum of 4 elements in the gaps were used; other parameter were left as default values. In addition, a custom control refinement for the domains with the contraction walls was used to create elements half of the general base size. The fans were modeled as squares with velocity inlet boundary conditions per fan. The outflow grid on the opposite wall was treated as uniform pressure outlet. All other surfaces were treated as no-slip

150   walls. Due to various values of the Reynolds number across the domain, controlling the wall y+ was challenging. Therefore, for modelling the Reynolds stresses in the RANS equations, two-layer K-epsilon (k-ε) turbulence model was chosen. The M1 setup at domain V and V-c were used for preliminary tuning of the input values at the inlets and the outlet boundary condition parameters in order to get the best match with the available data at the test section. The best results corresponded to an inlet turbulence intensity of 8% with length scale of 0.2 m and the outlet boundary set as a pressure outlet with uniform

155   zero-gauge pressure, 1% turbulence intensity and 0.05m length scale. Working at full power, the fans can generate 13 and 31 m/s velocity without and with contracting walls present at the test section respectively. In the end the results showed that the full fan powers corresponded to a 16.5 m/s inlet velocity. The fan power set-points were then simplified as a linear interpolation between 0 and 16.5 m/s for the velocity inlets.

160

165 **Table 2: Detail of grid sizes for each domain**

Grid name tag	M1	M2	M3
Number of Cells for Domain V (Million)	1.41	2.53	5.52
Number of Cells for Domain V-c (Million)	2.37	3.72	6.75
Number of Cells for Domain H (Million)	N/A	1.93	N/A
Number of Cells for Domain H-c (Million)	N/A	3.00	N/A
Base size (m)	0.1	0.08	0.06

The mesh independency check was defined by the incrementally refined grids M1 to M3 using the velocity profiles at the test section for the ABL profiles which have different fan power set points for each row (Figure 4). For low speed setup (without contraction) they were at 50, 70, 70 and 50% from bottom row to top (Figure 4a); for the setup with contractions,

170 the fans are at 50, 65, 75 and 75% (Figure 4b); The velocity profiles from the CFD results was defined by a probe line with 40 elements over the entire height of the chamber.

(a)   (b)
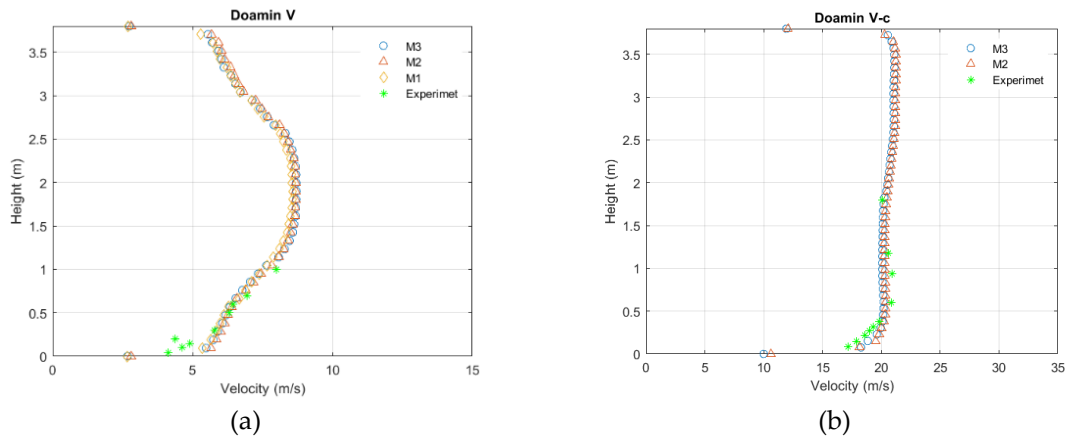
Figure 4. The mean ABL velocity profiles at the test section for different mesh setups comparing with the experimental data (Hangan et al., 2016)**, (a) low speed (without contraction) and (b) high speed (with contraction) mean velocity vertical profiles**

According to Figure 5a &b showing the relative errors between velocities at each height, the largest disconformities between different mesh setups occur close to the wall, which for this research is not the most important region. The more critical region for the present experiments is at the middle heights where the wind turbine rotor will be located. That being said, even

175 the M1 setup has an acceptable range of error at mid-height. However, the M2 mesh setup was chosen as the best compromise of computation speed and accuracy.

| (a) | (b) |
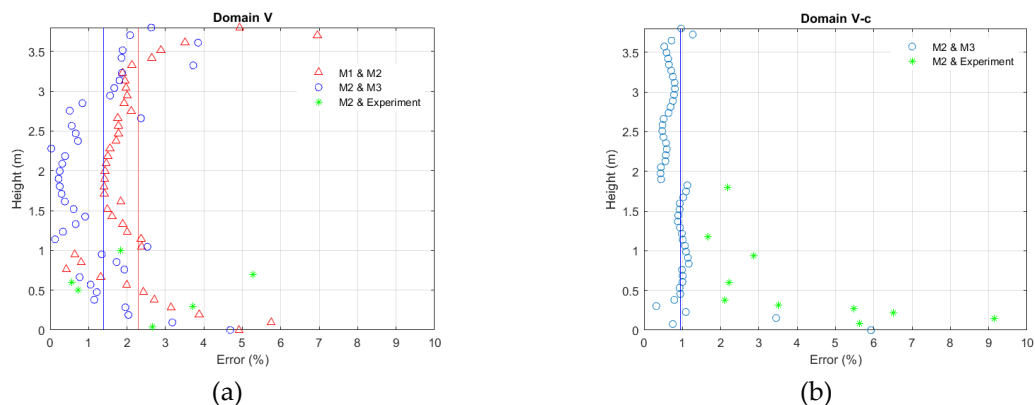
Figure 5. The relative errors for (a) low speed velocities and (b) high speed velocities, the solid lines are the mean value for the errors over the whole height

The discrepancy between the CFD simulation (M2) and the experimental data also increases close to the wall. This error is rooted in uncertainty of the implemented turbulence model and relative course mesh size close to the wall in the numerical model. Nevertheless, they are in an acceptable range of engineering applications (under 10% of relative error).

180   A picture of discretized domain V-c with the M2 grid is shown at Figure 6.
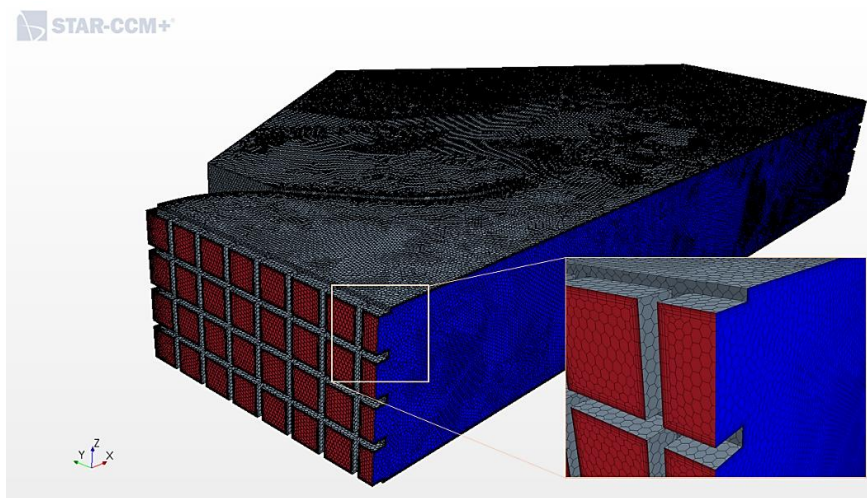
Figure 6. The M2 grid for the V-c domain

Finally, multiple runs for different uniform fan power set-points were conducted to make predictions about the relation between the fan power set-points and the velocity at the middle height of the test section (Table 3).

185

Table 3: The relation between fan powers and velocity at middle height of the test section, with and without contraction

Fan Power Set-Point (%)	Domain V-c, Velocity (m/s)	Domain V, Velocity (m/s)
10	3.1	1.3
20	6.2	2.6
30	9.3	3.9
40	12.4	5.2
50	15.5	6.5
60	18.6	7.8
70	21.7	9.1
80	24.8	10.4
90	27.9	11.7
100	31	13

2.3. Experimental setup for velocity measurements

The velocity measurements were obtained with seven cobra probes. Each probe has 4 pressure tabs at the head (0.5mm each)
and is able to measure three velocity components with measuring range from 2 to 45 m/s with ±0.5 m/s accuracy (Turbulent
Flow Instrumentation Pty Ltd). In this study the average wind velocity was 5 m/s, therefore all of the wind measurements
have ∼ 10% uncertainty in average.

Two different setups for velocity measurements were used: vertical and horizontal arrangements (Figure 7). The sampling
duration was 60 s with sampling frequency of 2000 Hz for each measurement run.

(a)   (b)
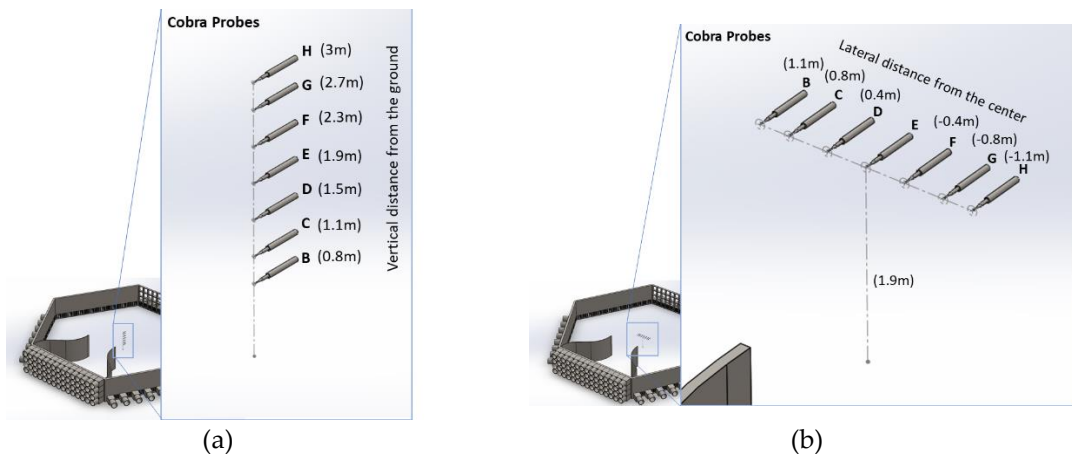
(c)

Figure 7. The arrangement of cobra probes based on the dimension of a 2.2m diameter HAWT for (a) vertical and (b) horizontal measurements at the center of the test section, (c) Setting up the 7 cobra probes in a horizontal arrangement at the test section

The location of the probes was chosen based on the dimension of the available wind turbine in the facility for future work. This turbine has a 2.2 m diameter with adjustable hub height, chosen as 1.9 m (Refan and Hangan, 2012).

2.4. Gust length and time scaling

200   The time duration of the gust (T), as mentioned earlier, is 10.5 s for a 1-year and 14 s for a 50-year return period in the IEC standard. The gust duration corresponds to 3 to 4 complete rotor revolutions periods for full-scale turbines, which for the scaled wind turbine in the wind tunnel would be on the order of a second at the nominal operating condition. This gust timescale would be impossible to simulate at WindEEE facility given the physical limitations of the hardware. Therefore, we assume that the time scale of the gust is equal to propagation time of 4 loops of a blade tip vortex downstream in the wake.

205   We can then calculate the propagation length and time of these vortex loops based on the definition of the TSR and assuming a uniform wake (Eq. (5)). The L' and T' are the length and time for one vortex loop in the wake.

$$\Omega = \frac{\lambda U}{R} [rad/s],$$

$$\Omega' = \frac{\lambda U}{R} \times \frac{1}{2\pi} [rev/s], \qquad (5)$$

$$U \times \frac{1}{\Omega'} = \frac{2\pi R}{\lambda} \left[\frac{m}{rev}\right],$$

Where Ω is the angular velocity, λ is TSR, U is the free stream velocity and R is the radius of the rotor. Which

210   can be rewritten as follow:

$$\frac{L'}{D} = \frac{T'U}{D} = \frac{\pi}{\lambda}, \qquad (6)$$

Based on the Eq. (6) and our assumption, an appropriate gust time and length can be calculated from:

$$\frac{L}{D} = \frac{TU}{D} = 4\frac{\pi}{\lambda},$$
(7)

Accordingly, the time scale is function of TSR, free stream velocity and the diameter of the rotor. The length scale is function of TSR and diameter of the rotor (Figure 8).

215 If the scaled turbine works at the same TSR and free stream velocity as the full-scale commercial HAWT, the time and length scale would be equal to their geometrical scale (i.e. the ratio of diameters).
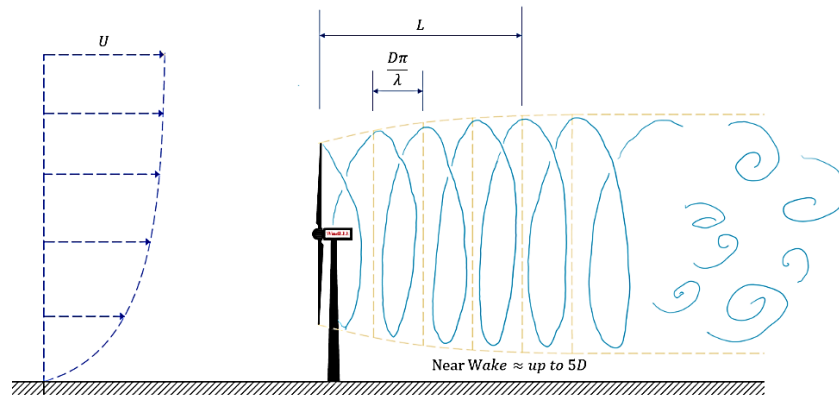
Figure 8. Visual representation of the length and the time scale proper for the extreme conditions with assuming a symmetric wake

The flow behaviour in the near wake region is directly correlated to the overall performance of a HAWT (Hashemi Tari et al., 2016). Matching the time duration of the extreme condition to the propagation of 4 vortex loops in the wake should be a reasonable comparison to the full scale in terms of variation of power and loads on the wind turbine. The physical

220 experiments showed that the fastest possible gust events with the required peak factor were at time scales of 5 seconds due to the hardware limitation. Therefore, based on our assumption, this requires the 2.2m scaled wind turbine to work in 5m/s free stream velocity with operating TSR of 1.1 then it would take 5 seconds for the four complete loops of the tip vortexes generated by a specific blade to propagate in the wake. Accordingly, in all of the simulations and experiments the hub height velocity was kept at 5 m/s to increase the overall time scales. The Reynolds number calculated from the relative velocity and

225 chord size at 70% span of the blade for full scale turbine at the nominal wind speed and TSR (10 m/s and 8 respectively) is $\sim 7.5 \times 10^6$ and for the scaled turbine at the our lab condition is $\sim 32.5 \times 10^3$ which gives the ratio of ~ 230. This mismatch can be improved by using higher density fluids or being capable of running the experiment at higher wind velocities and TSRs. In this setup, the ratio of the length and time scale become 5.23 and 2.61 respectively.

230 All of the simulations and experiments were tailored for the available scaled wind turbine. Assuming a similar B-III class HAWT with hub height of ~10 m for the 2.2 m rotor, the extreme condition profiles look identical to the full-scale ones (the same peak factor but different gust time) at 5 m/s average hub-height velocity considering 1-year return period, as it is shown in Figure 9.

Accordingly, for the EOG the velocity should uniformly rise from 5 to 9.5 and then back to the 5 m/s in 5 seconds with ~1.5
235 m/s drop before and after the main peak relative to the average free stream velocity (Figure 9a), however, in experiments the gusts have been simplified by ignoring the velocity drops.

For the EVS the uniform velocity field transitions to a highly sheared flow (~7 m/s velocity shear in 2.2 m distance) and then back to a uniform field, again in 5 seconds (Figure 9b). For the full scale the same amount of velocity difference happens over 92 m with different time scale.

(a)   (b)
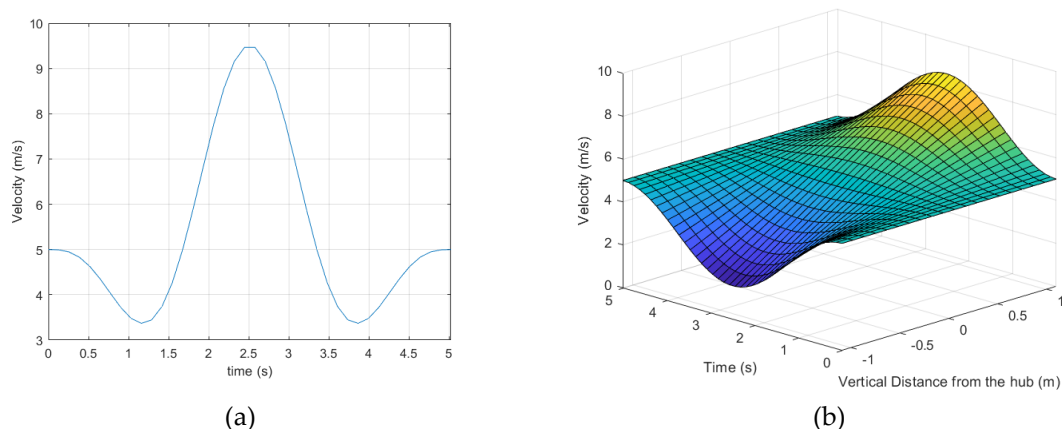
Figure 9. The target extreme conditions for simulations and experiments based on the scaled wind turbine and capability of the fans, identical to prescribed extreme condition for the full-scale wind turbine just with different time scale, (a) extreme operating gust, (b) extreme vertical shear

240 ## 3. Results and discussion

3.1. Steady wind shear

In this section the simulation cases are all steady and just for the peak stage which is the instantaneous point in time that maximum shear occurs, as a preliminary investigation to unsteady experiment runs that examined in the next sub-section. Using the tuned numerical model setups, the V-c and H-c domains were used to generate the desired vertical and horizontal
245 sheared flows by manipulating the input velocity for the different rows and columns of the fans. The target was to match as closely as possible the velocity profile to the IEC standard for the scaled HAWT, corresponding to ~7 m/s shear while keeping the velocity at the rotor centerline 5 m/s. Figure 10 shows the fan setups using CFD for creating the desired shears which could be achieved by using only the 5 fan columns at the middle. For creating negative vertical shear, the setup presented in Figure 10a was inverted.

(a)   (b)
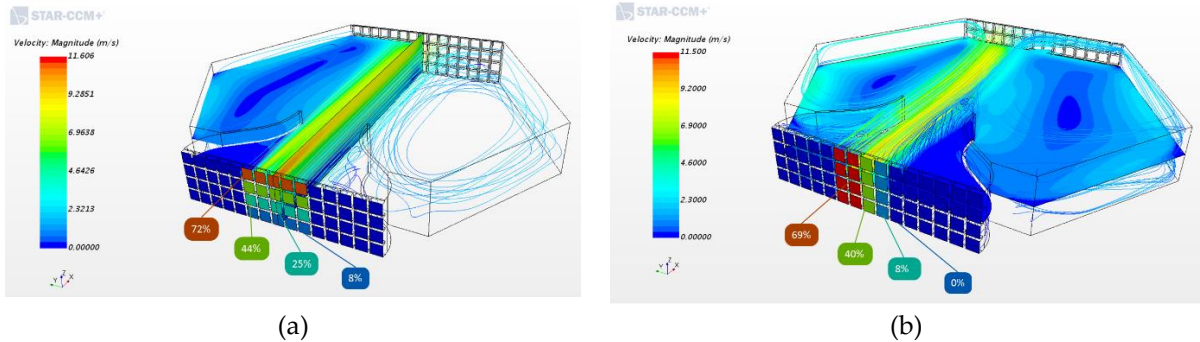
Figure 10. Fan setups for peak stages of extreme (a) vertical and (b) horizontal shears, prescribed for the scaled HAWT identical to full scale condition, the power set-points for each row and columns is included (just the 5 columns at the middle are working)

250

Using the fan setups shown in Figure 10 the physical experiment was carried out and velocity measurements made using the Cobra probes. Figure 11 shows the average velocity at each probe including the range of standard deviation compared with average velocity profile from the CFD and the prescribed shear by IEC standard. These high amount of velocity deviations relative to the mean velocity are due to the strong vortexes that form in these highly sheared and unstable flows that increase

255 the momentum mixing at different heights. From Figure 11a & c it is clear that the lower fans work more efficiently than the upper fans; i.e. with the same value of the power set-point, the lower fans generate higher velocities. The largest error exists in the horizontal shear case (Figure 11 b). The relative difference between the mean velocities from experimental data with IEC standard (Eq. (8)) is presented at Figure 11 d.

$$Relative\ Error(i) = \left| \frac{\overline{U}_{Experiment}(i) - U_{IEC}(i)}{U_{IEC}(i)} \right| \times 100, \qquad (\ 8)$$

260

The amount of shear that was prescribed (~7 m/s velocity difference) is being successfully created in the tunnel for the positive vertical shear case. However, for the horizontal and negative vertical cases there is a larger than desired shear, resulting in an ~10 m/s velocity difference which can be adjusted in future.
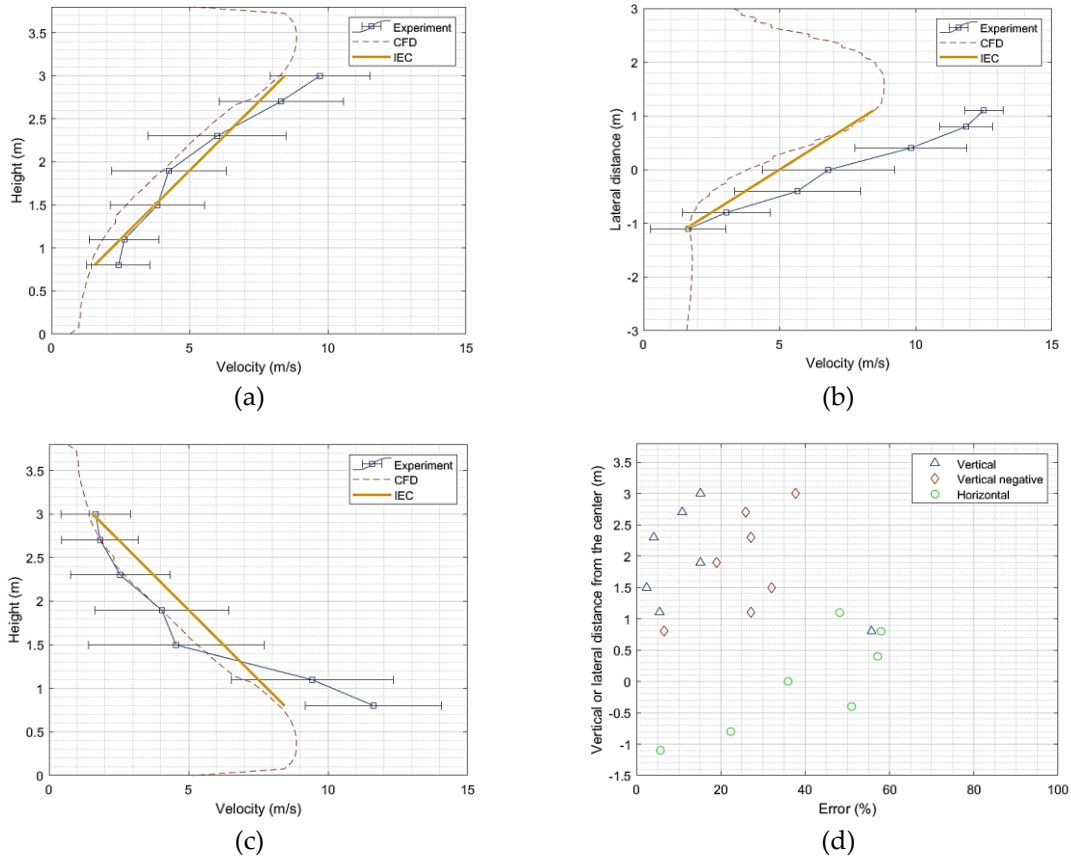
Figure 11. CFD predictions vs experiment data for steady (a) vertical shear, (b) horizontal shear and (c) negative vertical shear, (d) the relative error between experiment and IEC standard

265

3.2. Unsteady experiments

As mentioned earlier, it is possible to control the fans with a spread sheet file. The switching time between each row in the file of power set-points was chosen as 0.8s. For the shear cases just the five columns of fans in the middle were working. For the nominally uniform inflow condition, in the beginning and the end of the shear events, they were all set at 39% power.

270 The best results in terms of time scale and peak factor were obtained when 2 rows of extreme condition power set-points (the setup at Figure 10) was used in the file. Therefore, the file has many rows of 39% in all the sixty columns and then at certain point just two rows of the extreme condition fan setups. The uniform gusts were generated in two ways. The first was again by changing the power set-points of the fans together. According to the results from the CFD simulations (Domain V-c), in order to achieve the prescribed EOG, the fan power set-points should uniformly go from 17% to 30% (correspond to 5 and

275 9.3 m/s wind at test section) and back to the 17% power. For the uniform gust the best result again obtained with having 2 rows of extreme condition power set-points in the spread sheet file which resulted in $\sim 5\ s$ uniform gust with desired peak

factor. For example if we put the fan power setups for the extreme condition at the 11th and 12th row in the file, the event start happening ~8s after the software start reading the file (considering 0.8s switching time between rows).The second way of generating a uniform gust was using the IGVs while keeping fan power set-points constant at 30%. In this run, the

280 actuation frequency of the IGVs was set at 0.05 Hz with a duty cycle of 8%, initial position of 10% open with cycling to 100% open (see section 2.1 for IGV setting definitions). In addition, for each uniform gust case, two runs were conducted in order to measure the velocity field with both vertical and horizontal layouts of the cobra probes in order to investigate the uniformity of the inflow. All of the velocity time histories were filtered using a moving average. The best results were obtained when the moving average window was 0.2 s based on the criteria described at (Chowdhury et al., 2018).

285 3D pictures of the filtered turbulent wind fields for the EVS, EHS, negative EVS, EOG cases generated with changing fan powers (vertical & horizontal measurements), and the EOG generated using the IGVs (vertical & horizontal measurements) are presented in Figure 12a, b, c, d & e, f & g respectively.
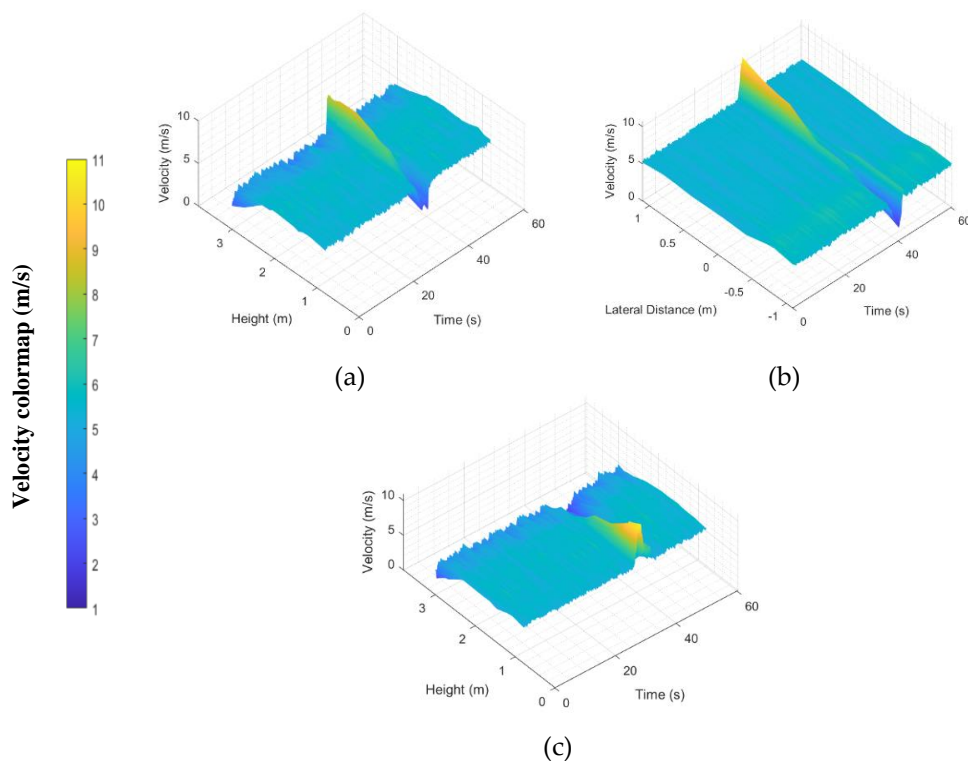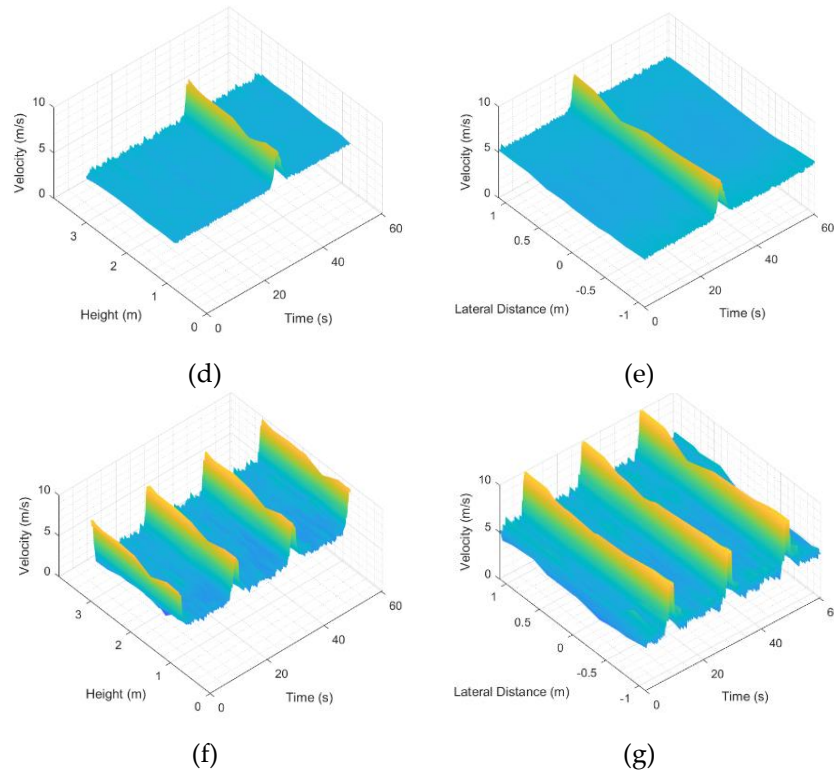
Figure 12. 3D pictures of the complete time history of the filtered turbulent velocity field, (a) EVS, (b) EHS, (c) negative EVS, EOG generated with changing fan powers (d) vertical (e) horizontal measurements, EOG generated with IGVs (f) vertical (g) horizontal measurements

In order to have a better comparison of the generated extreme unsteady cases with what the standard prescribes, the velocity time history extracted from each cobra probe (blue solid line) with the layout showed in Figure 7, as well as what the standard suggests (in orange solid line) are plotted in Figure 13 in the left columns (the cases are in the same order as Figure 12). The right column contains the relative instantaneous discrepancy of the velocity to the IEC prescribed velocity, normalized by the average velocity ($\sim 5 \; m/s$) as Eq. (9):

$$Relative \; Error(t) = \left| \frac{U_{experiment}(t) - U_{IEC}(t)}{\bar{U}} \right| \times 100. \tag{9}$$

Based on data for the shear cases, at the peak stages the amount of desired shear is successfully being generated. However, due to the difference in velocities, there is a time lag between the peaks at the top to bottom heights of the EVS cases, and left to right in the EHS cases (Figure 13a, b and c).
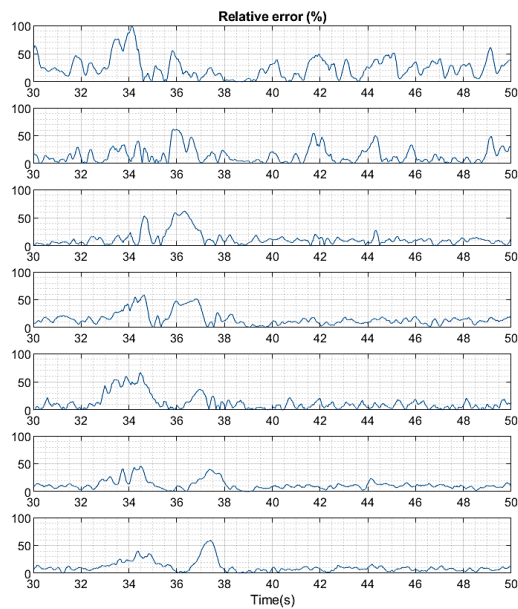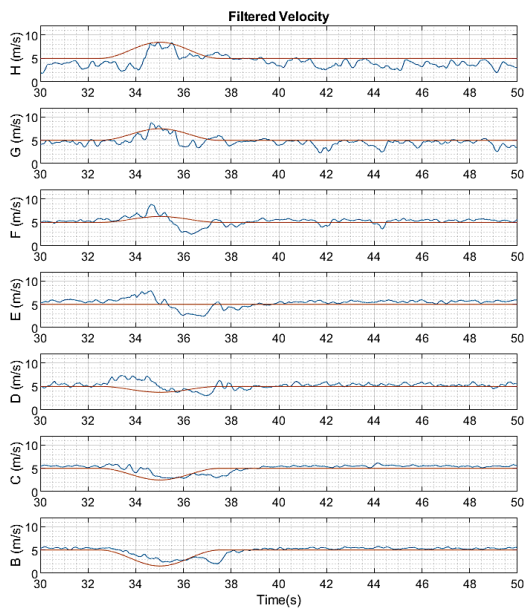
(a)
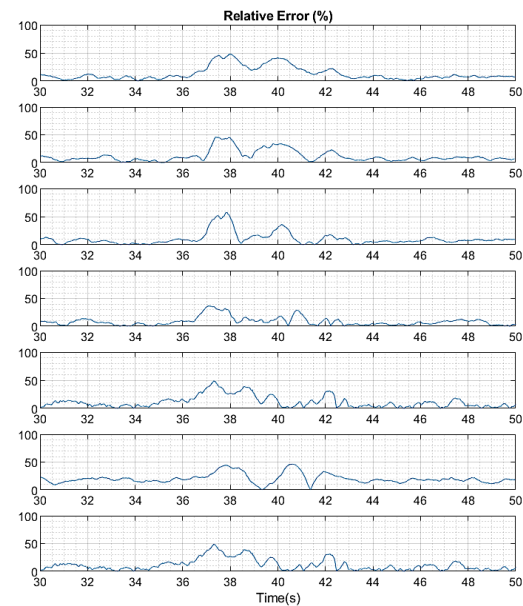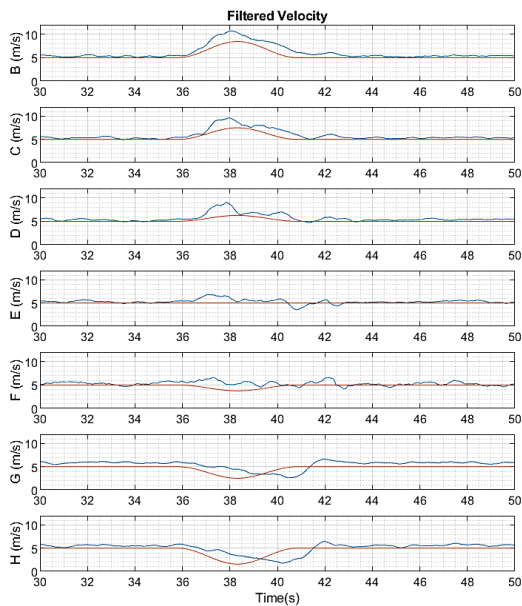
(b)
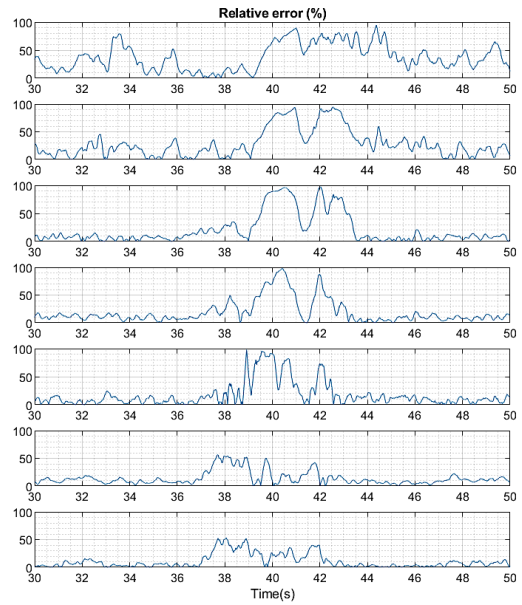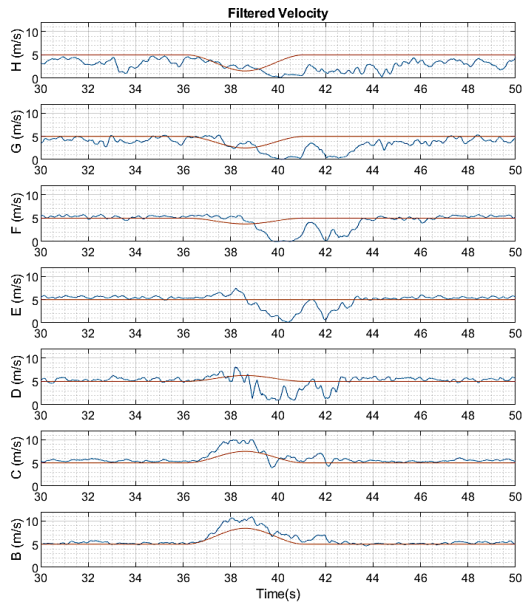
(c)
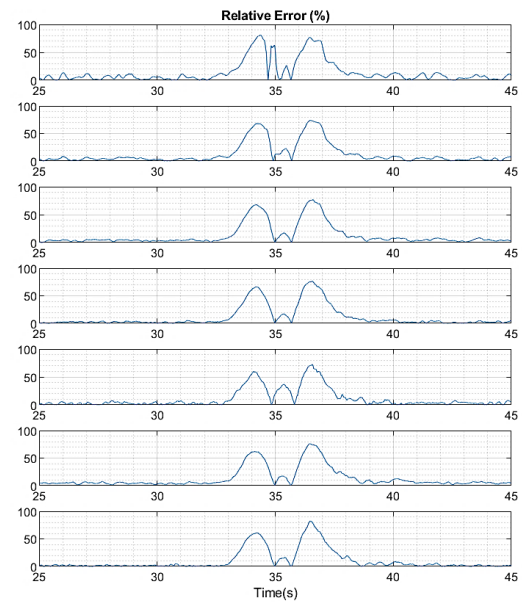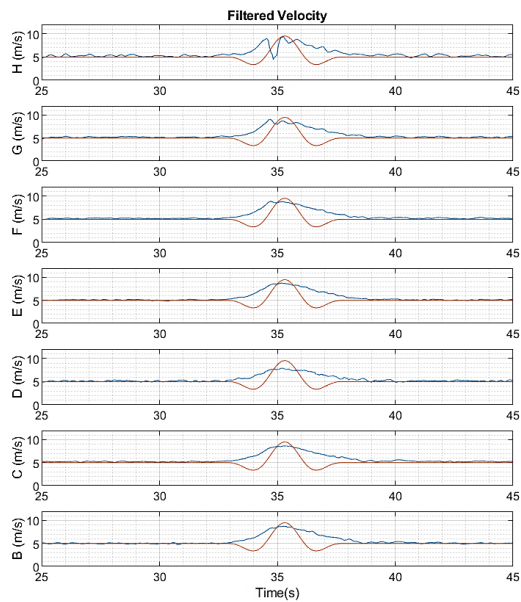
(d)

(e)

(f)

(g)
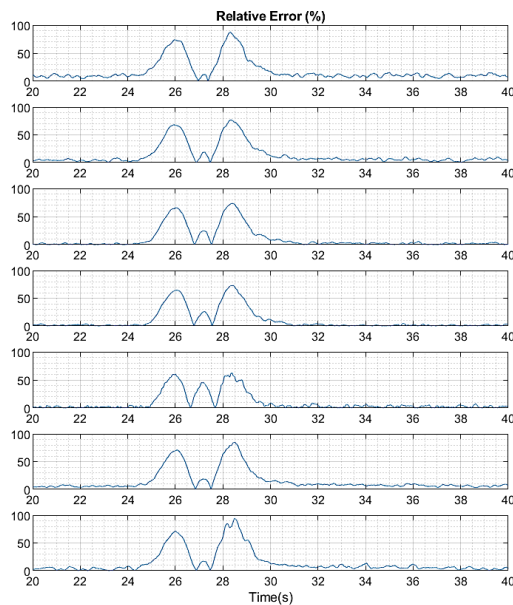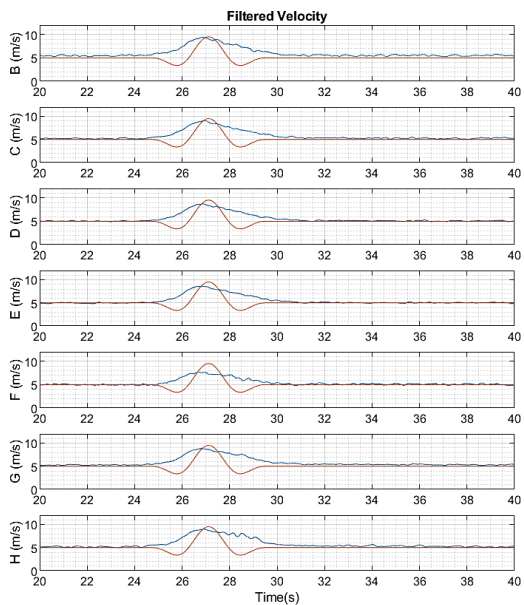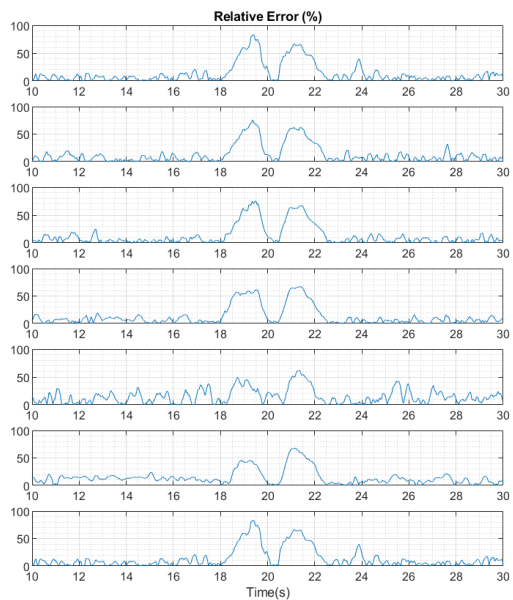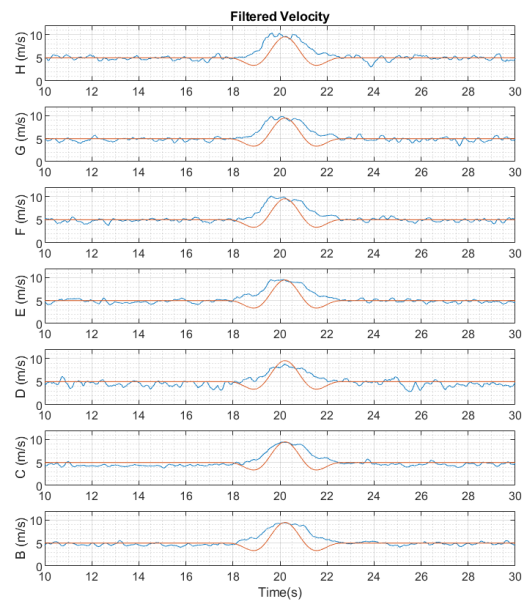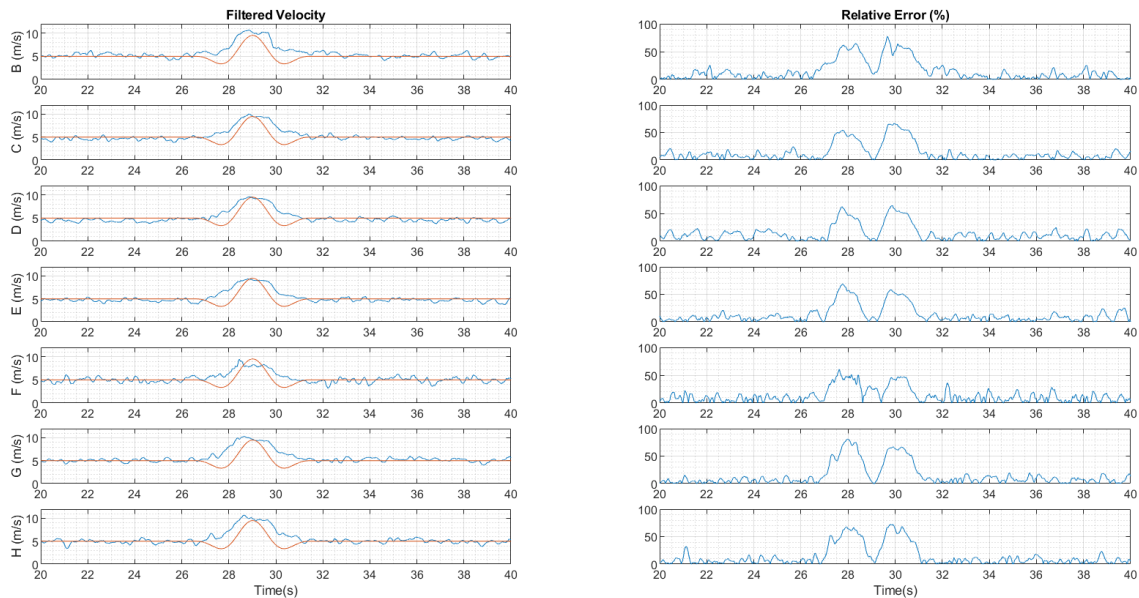
Figure 13. Filtred velocity time history at each probe (with the layout presented in Figure 7) as solid blue line compared with prescribed extreme velocity as a solid orange line (left column), time history of relative instantaneous velocity discrepancy normalized by average velocity (right column) for (a) EVS, (b) EHS, (c) negative EVS, EOG generated with changing fan powers (d) vertical and (e) horizontal measurements, EOG generated with IGVs (f) vertical and (g) horizontal measurements

300   Based on Figure 13d for the EOG generated with changing fan powers, the velocity at the upper height in the test section is not achieving a totally uniform flow condition (time series from probe H). However, the desired peak factor has been generated. The most consistent uniform gust was generated using IGVs, in terms of uniformity and peak factors at the test section, at least in the measurements area (Figure 13f & g). The only noticeable discrepancy for the EOG generated with the IGVs is due to the small drop in velocity before and after the main rise of velocity in the prescribed gust case, which created

305   dual peaks in the relative error time history. If we simplify the standard gust profile and ignore the velocity drops, the generated gusts with this method would look identical to the theory.

4. Conclusion

A numerical and experimental study has been carried out to investigate the possibility of creating extreme conditions for a

310   scaled HAWT based on the IEC 61400-1 standard, in particular the EOG, EVS and EHS cases, using the unique 60 fan setup in the WindEEE dome. These conditions were tailored for a 2.2 m diameter scaled HAWT. The aim was to relate this work to full-scale wind turbines. Therefore, a simple length and time scaling based on tip vortex propagation in the wake was

presented. Based on that approach, the duration of each extreme condition was set equal to four tip vortex loops propagating downstream. Accordingly, the time scale is a function of the free stream velocity, tip speed ratio and diameter of the rotor.

315   The tuned and validated numerical simulations of tunnel operation gave a good understanding of the relation between fan power set points and the flow field in the relevant part of test chamber. It also gave insight into the interaction of the free shear layers for non-uniform fan setups prior to running the experimental campaigns.

The steady experiment runs corresponding to the peak of the shear cases shows the fans act non-linearly and they have different individual efficiencies, especially the top and bottom rows despite our simplified assumptions for developing the

320   CFD model. However, excluding the top and bottom rows the errors are in an acceptable range (∼ 10% relative error in average) compared with the IEC standard. By knowing these discrepancies corrections can be applied to the fan inputs and make the shears as identical as possible to the standard. The unsteady shear flow experiments showed that the flow field is more distorted due to the differences in speed generated at the fans. There is a time lag between the highest and lowest peak, which also can be corrected in future by giving a phase difference in actuations between the top and bottom rows. But more

325   importantly the desired peak factor overall has been captured.

Generating uniform gusts using the IGVs, produced the best results in terms of time scale and peak factors as well as flow field uniformity. By ignoring the sudden velocity drops in the theoretical gust profile, the generated gusts would become identical to the standard. The results from changing fan power set-points were consistent as well. However, due to flow recirculation from the top and then behind the fans, the top row of fans does not work as efficient as other 3 rows in high

330   transition in power set-points which resulted on a little non-uniformity at top heights of the test chamber. The same problem that mentioned for creating shears.

Overall, this study demonstrated a successful simulation of extreme wind conditions, which can now be used for future experimental tests to investigate their effects on different aspects of wind turbine performance with minor modifications. The developed numerical model can be similarly used in the future to obtain the primary fan setups prior to experiment for

335   different target scenarios at the test section.

Authors contributions

KS developed the numerical model and the scaling with direct supervision from CC. KS carried out all the experiments with supervision of HH. KS wrote the main body of the paper with input from all authors.

340   **Competing interests**

The authors declare that they have no conflict of interest

Acknowledgements

All authors thank Gerald Dafoe and Tristan Cormier for helping with the measurement setups. The present work is supported by UWO and the IESVic.

345 **References**

Bossanyi, E. A., Kumar, A. and Hugues-Salas, O.: Wind turbine control applications of turbine-mounted LIDAR, in Journal of Physics: Conference Series, vol. 555, Institute of Physics Publishing., 2014.

Cheng, P. and Bierbooms, W.: Extreme gust loading for wind turbines during operation, in 20th 2001 ASME Wind Energy Symposium, American Institute of Aeronautics and Astronautics, Reston, Virigina., 2001.

350 Chowdhury, J., Chowdhury, J., Parvu, D., Karami, M. and Hangan, H.: Wind flow characteristics of a model downburst, in American Society of Mechanical Engineers, Fluids Engineering Division (Publication) FEDSM, vol. 1, American Society of Mechanical Engineers (ASME)., 2018.

Gharali, K. and Johnson, D. A.: Effects of nonuniform incident velocity on a dynamic wind turbine airfoil, Wind Energy, 18(2), 237–251, doi:10.1002/we.1694, 2015.

355 González-Longatt, F., Wall, P. P. and Terzija, V.: Wake effect in wind farm performance: Steady-state and dynamic behavior, Renew. Energy, 39(1), 329–338, doi:10.1016/j.renene.2011.08.053, 2012.

Hangan, H., Refan, M., Jubayer, C., Parvu, D. and Kilpatrick, R.: Big data from big experiments. The WindEEE Dome, in Whither Turbulence and Big Data in the 21st Century?, pp. 215–230, Springer International Publishing., 2016.

Hangan, H., Refan, M., Jubayer, C., Romanic, D., Parvu, D., LoTufo, J. and Costache, A.: Novel techniques in wind
360 engineering, J. Wind Eng. Ind. Aerodyn., 171, 12–33, doi:10.1016/j.jweia.2017.09.010, 2017.

Hansen, M.: Aerodynamics of wind turbines., 2015.

Hashemi Tari, P., Siddiqui, K. and Hangan, H.: Flow characterization in the near-wake region of a horizontal axis wind turbine, Wind Energy, 19(7), 1249–1267, doi:10.1002/we.1895, 2016.

Hu, W., Letson, F., Barthelmie, R. J. and Pryor, S. C.: Wind Gust Characterization at Wind Turbine Relevant Heights in
365 Moderately Complex Terrain, J. Appl. Meteorol. Climatol., 57(7), 1459–1476, doi:10.1175/JAMC-D-18-0040.1, 2018.

Jeong, M., Kim, S., Lee, I., Structures, S. Y.-J. of F. and and 2014, undefined: Wake impacts on aerodynamic and aeroelastic behaviors of a horizontal axis wind turbine blade for sheared and turbulent flow conditions, Elsevier, n.d.

Lackner, M. A. and Van Kuik, G. A. M.: The performance of wind turbine smart rotor control approaches during extreme loads, J. Sol. Energy Eng. Trans. ASME, 132(1), 0110081–0110088, doi:10.1115/1.4000352, 2010.

370 Micallef, D. and Sant, T.: Rotor aerodynamics in sheared inflow: An analysis of out-of-plane bending moments, in Journal of Physics: Conference Series, vol. 1037, Institute of Physics Publishing., 2018.

Pace, A., Johnson, K. and Wright, A.: Preventing wind turbine overspeed in highly turbulent wind events using disturbance accommodating control and light detection and ranging, Wind Energy, 18(2), 351–368, doi:10.1002/we.1705, 2015.

Patlakas, P., Diamantis, D., Galanis, G. and Kallos, G.: Towards a Study of Different Types of Extreme Wind Speed

375   Conditions, pp. 421–427., 2017.

Peinke, J., Anahua, E., Boettcher, F., Barth, S. and Lange, M.: Stochastic analysis of the power output for a wind turbine., n.d.

Refan, M. and Hangan, H.: Aerodynamic performance of a small horizontal axis wind turbine, J. Sol. Energy Eng. Trans. ASME, 134(2), doi:10.1115/1.4005751, 2012.

380   Schlipf, D., Schlipf, D. J. and Kühn, M.: Nonlinear model predictive control of wind turbines using LIDAR, Wind Energy, 16(7), 1107–1129, doi:10.1002/we.1533, 2013.

Sezer-Uzol, N. and Uzol, O.: Effect of steady and transient wind shear on the wake structure and performance of a horizontal axis wind turbine rotor, Wind Energy, 16(1), 1–17, doi:10.1002/we.514, 2013.

Shen, X., Zhu, X., Energy, Z. D.- and 2011, undefined: Wind turbine aerodynamics and loads control in wind shear flow,

385   Elsevier, n.d.

Snel, H., Schepers, J. G. and Montgomerie, B.: The MEXICO project (Model Experiments in Controlled Conditions): The database and first results of data processing and interpretation, in Journal of Physics: Conference Series, vol. 75., 2007.

Sørensen, N. N., Michelsen, J. A. and Schreck, S.: Navier-Stokes predictions of the NREL phase VI rotor in the NASA Ames 80 ft × 120 ft wind tunnel, Wind Energy, 5(2–3), 151–169, doi:10.1002/we.64, 2002.

390   Suomi, I., Vihma, T., Gryning, S.-E. and Fortelius, C.: Wind-gust parametrizations at heights relevant for wind energy: a study based on mast observations, Q. J. R. Meteorol. Soc., 139(674), 1298–1310, doi:10.1002/qj.2039, 2013.

Thomsen, K. and Sørensen, P.: Fatigue loads for wind turbines operating in wakes, J. Wind Eng. Ind. Aerodyn., 80(1–2), 121–136, doi:10.1016/S0167-6105(98)00194-9, 1999.

Tony Burton, Nick Jenkins, David Sharpe, E. B.: Wind Energy Handbook, 2nd Ed., WILEY., 2011.

395   Ueckerdt, F., Hirth, L., Luderer, G. and Edenhofer, O.: System LCOE: What are the costs of variable renewables?, Energy, 63, 61–75, doi:10.1016/j.energy.2013.10.072, 2013.